Inorganic Chemistry

Article

pubs.acs.org/IC

Synthesis, Characterization, and Photophysical Studies of an Iron(III) Catecholate−Nitronylnitroxide Spin-Crossover Complex

Christopher R. Tichnell,[†] David A. Shultz,*[,†] Codrina V. Popescu,*[,‡] Ivan Sokirniy,[⊥] and Paul D. Boyle[†,§]

[†]Department of Chemistry, North Carolina State University, Raleigh, North Carolina 27695-8204, United States

[‡]Department of Chemistry, Colgate University, 13 Oak Drive, Hamilton, New York 13346, United States

[⊥]Department of Chemistry, Ursinus College, Collegeville, Pennsylvania 19426, United States

Supporting Information

ABSTRACT: The synthesis and characterization of an Fe^{III} catecholate−nitronylnitroxide (CAT-NN) complex (**1-NN**) that undergoes Fe^{III} spin-crossover is described. Our aim is to determine whether the intraligand exchange coupling of the semiquinone−nitronylnitroxide Fe^{II}(SQ-NN) excited state resulting from irradiation of the CAT → Fe^{III} LMCT band would affect either the intrinsic photophysics or the iron spin-crossover event when compared to the complex lacking the nitronylnitroxide radical (**1**). X-ray crystallographic analysis provides bond lengths consistent with a ferric catecholate charge distribution. Mössbauer spectroscopy clearly demonstrates Fe^{III} spin-crossover, hyperfine couplings, and a weak ferromagnetic Fe^{III}−CAT-NN exchange, and spin-crossover is corroborated by variable-temperature magnetic susceptibility and electronic absorption studies. To explore the effect of the NN radical on photophysical processes, we conducted room-temperature transient absorption experiments. Upon excitation of the ligand-to-metal charge transfer band, an Fe^{II}SQ state is populated and most likely undergoes fast intersystem crossing to the ligand field manifold, where it rapidly decays into a metastable low-spin Fe^{III}CAT state, followed by repopulation of the high-spin Fe^{III}CAT ground state. The decay components of **1-NN** are slightly faster than those obtained for **1**, perhaps due to the higher number of microstates present within the LMCT and LF manifolds for **1-NN**. Although the effects of the NN radical are manifest in neither the spin-crossover nor the photophysics, our results lay the groundwork for future studies.

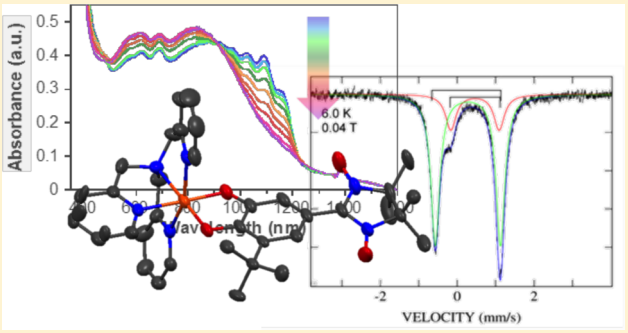

INTRODUCTION

Catechols, semiquinones, and quinones, members of the dioxolene ligand redox series, have been actively explored for decades due to their redox noninnocence.[1] This redox activity has led to the use of dioxolenes in bioinorganic research,[2] electron transfer studies,[3] valence tautomerism,[4,5] metal complexes of paramagnetic ligands,[6,7] and mixed-valent complexes.[3,8] Ferric catecholates are prominent examples of dioxolene-containing metal complexes that serve as functional models of diol cleavage enzymes.[2]

Recent studies involving ferric catecholates, with ties to diol cleavage, involve analyzing the electronic structure of the low-energy doublet (*ls*-Fe^{III}CAT, $S = 1/2$) and sextet (*hs*-Fe^{III}CAT, $S = 5/2$) "ground" states of the observed thermal equilibrium spin-crossover (SCO).[9,10] These states possess dioxolene−metal charge transfer (typically LMCT) character, resulting in a ground state having both Fe^{III}(catecholate) (Fe^{III}Cat) and Fe^{II}(semiquinone) (Fe^{II}SQ) contributions due to configuration interaction.[9,11,12] This has been shown experimentally in [(TPA)Fe^{III}(CAT)] (TPA = tris(2-pyridylmethyl)amine) through decreased anisotropy in the *ls*-Fe^{III}CAT $S = 1/2$ EPR spectrum, indicating greater Fe^{II}SQ character.[13] Enhanced Fe^{II}SQ character in the ground state has also been correlated with bathochromic shifts in the LMCT bands observed spectroscopically,[11,13] which corresponds to greater π-covalency. Finally, pump−probe photoexcitation experiments have been performed on [(TPA)Fe^{III}(CAT)] complexes at $T < 100$ K to assess *ls* to *hs* light-induced excited spin state trapping (LIESST)[14] tunneling phenomena.[15]

An emerging area of "chemical spintronics"[16] research is the study of excited states having pendant radical spin(s). Over the last two decades, Wasielewski and Teki have studied photoexcitation of ground-state paramagnetic stable radical systems. Their work has shown that radical-appended chromophores undergo enhanced intersystem crossing relative to the non-radical appended chromophores[17,18] and that exchange interactions between charged-separated, paramagnetic chromophore fragments and the pendent radical provide spin-polarization mechanisms that alter charge recombination rates.[19−21] Moreover, recent work has been done by Teki to probe how photogenerated ligand-localized spin can affect metal-based processes such as SCO and valence tautomerism.[22,23]

Received: February 9, 2015
Published: April 16, 2015

DOI: 10.1021/acs.inorgchem.5b00298
Inorg. Chem. 2015, 54, 4466−4474

Given the demonstrated $Fe^{II}SQ$ LMCT excited-state contribution to ground-state reactivity and spectroscopy of $Fe^{III}CAT$ complexes, we hypothesized that covalent attachment of a stable radical (e.g., nitronylnitroxide = NN) to the CAT ligand would result in an LMCT excited state with the $Fe^{II}SQ$-NN charge distribution and strong ferromagnetic SQ-NN exchange,[24] which could affect either the excited-state photophysics, the Fe^{III} SCO, or both. This hypothesis was based on our previous studies of strong ferromagnetic SQ-NN exchange observed in several metal complexes of this and related ligands.[7,24,25]

In this work, we present a comparative study between $[(TPA)Fe^{III}(CAT\text{-}NN)]BPh_4$ (**1-NN**) and $[(TPA)Fe^{III}(3,5\text{-}DBCAT)]BPh_4$ (**1**) (where CAT-NN = 3-*tert*-butyl-5-nitronylnitroxidecatecholate and 3,5-DBCAT = 3,5-di-*tert*-butylcatecholate) shown in Figure 1. This study utilizes a gamut of

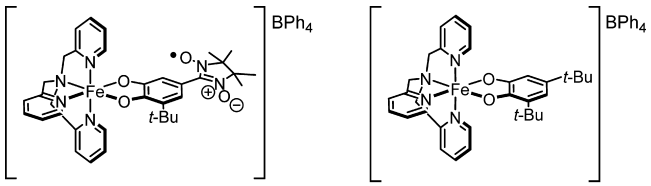

$[(TPA)Fe^{III}(CAT\text{-}NN)]BPh_4$ **(1-NN)** $[(TPA)Fe^{III}(3,5\text{-}DBCat)]BPh_4$ **(1)**

Figure 1. Bond line drawings of ferric catecholate complexes in this study.

spectroscopies, electrochemistry, and magnetometry to describe the electronic structure with respect to the magnetic properties and excited-state dynamics. The goal of this study is to assess the differences between these two complexes where one expectedly contains a strongly coupled photogenerated SQ-NN biradical in the LMCT excited state. The presence of the NN spin is expected to increase the manifold states and alter their energies relative to **1**, which could lead to notable changes in the electronic structure since those states could hypothetically result in additional superexchange pathways and decay mechanisms.

RESULTS AND DISCUSSION

Synthesis and Characterization. Complexes **1-NN** and **1** were prepared through one-pot reactions commonly used for synthesizing $(TPA)Fe^{III}(CAT)$ complexes.[11,26] In this procedure, H_2CAT-NN or 3,5-DBCATH_2 and two equivalents of triethylamine were added to a solution of ferric chloride and TPA ligand. Coordination of the CAT ligand was accompanied by a color change from yellow to dark violet. After stirring for 2.5 h, a methanol solution of $NaBPh_4$ was added to induce precipitation. Performing the reaction with dilute solutions resulted in air-stable microcrystalline solids that formed upon standing for several weeks. Complexes **1-NN** and **1** exhibited visual signs of decomposition while in solution especially in the presence of oxygen.

X-ray quality crystals of complex **1-NN** were obtained from the dilute methanolic reaction mixture. A thermal ellipsoid plot of MeOH-solvated **1-NN** (**1-NN·MeOH**) is shown is Figure 2, and crystallographic parameters and select bond lengths and angles are presented in the Supporting Information. The structure of **1-NN·MeOH** contains one BPh_4 anion consistent with the unit +1 charge of the $[(TPA)Fe(CAT\text{-}NN)]$ cation. The CAT C−O bond lengths (1.351 and 1.348 Å) and nearly

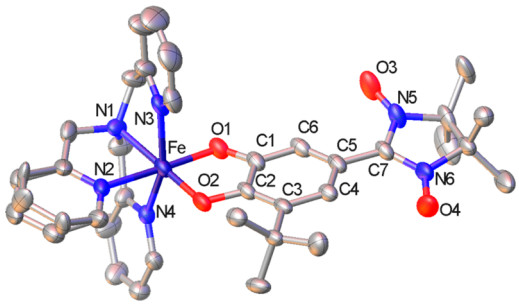

Figure 2. X-ray structure of **1-NN·MeOH** cation at 110 K with 50% probability ellipsoids. MeOH solvate, BPh_4 counterion, and hydrogens are removed for clarity. Distortion in both TPA and BPh_4 was observed; see Supporting Information.

symmetric C−C bond lengths allow for assigning the dioxolene ligand as a dianionic catecholate. Given the complex cation and ligand charges, the metal center is identified as Fe^{III}. The difference between C−O bond lengths is 0.0030 Å, but for **1** that difference is 0.019 Å.[27] Compared to the Fe−O bond lengths (1.917 and 1.898 Å) of **1**,[27] the Fe−O bond lengths (1.904 and 1.901 Å) of **1-NN·MeOH** are shorter, indicating stronger coordination of the NN-CAT ligand relative to 3,5-DBCAT. The Fe−N(amine) bond length is 2.130 Å, and the Fe−N(pyridyl) bond lengths vary from 2.064 to 2.087 Å. Assigning *ls* or *hs* configuration based upon these values cannot be done since the Fe−N and Fe−O bond lengths do not trend toward either configuration typical of $[(TPA)Fe(CAT\text{-}R)]$[13] or $Fe^{III}N_4O_2$ coordination[28] complexes. The torsion angle between CAT and NN is 17°, which is similarly seen for SQ-NN biradicals.[6,7] The distance between the Fe center and NN is approximately 6.4 Å. Compared to other Fe-NN complexes, this intramolecular distance ranges from almost 2- to 3-fold greater.[29,30] The shortest Fe−NN and NN−NN intermolecular interaction is 6.271 and 5.963 Å, respectively, which allows for ruling out intermolecular interactions in magnetic data interpretations.[31,32]

Variable-Temperature Mössbauer Spectroscopy. Given that **1** has been reported to undergo SCO,[12] Mössbauer spectra of **1-NN** in a 0.04 T magnetic field were collected at temperatures ranging from 5 to 295 K to evaluate potential SCO equilibrium. The 0.04 T spectra at 5 and 6 K exhibit two partially resolved quadrupole doublets. The major species, with an isomer shift of 0.29 mm/s, accounts for 78% of the Fe^{III} in the sample. This doublet was assigned as the *ls*-Fe^{III} component of the complex **1-NN**. A minority species with 22% relative area has an isomer shift of 0.46 mm/s and ΔE_Q = 1.26 mm/s (inside shoulder in Figure 3) and was assigned as the *hs*-Fe^{III} component. These isomer shifts are in the ranges expected for low-spin and high-spin Fe^{III} complexes with nitrogen/oxygen coordination.[33] The assignment of the spectral lines to each component (*ls* and *hs*, respectively), shown by the brackets in Figure 3, is based on the evolution of the relative ratio of these two doublets between 5 and 180 K and is in agreement with the parameters determined from the high-field spectra (see below). The spectra at 6 K were sharp and free of impurities, and the simulations and least-squares fits match the experimental spectra very well.

Increasing the temperature led to an increase in the relative area of the high-spin component and a corresponding decrease of that of the low-spin component (Figure 4). On the basis of the simulations of the Mössbauer spectra the temperature for

DOI: 10.1021/acs.inorgchem.5b00298
Inorg. Chem. 2015, 54, 4466−4474

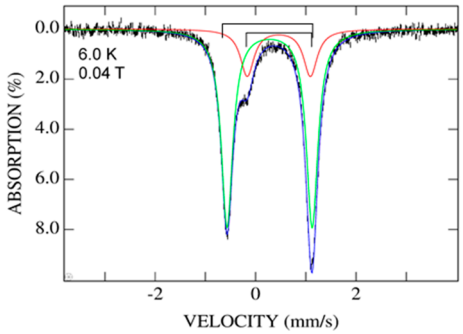

Figure 3. The 6 K spectrum of **1-NN** in a 0.04 T applied magnetic field. The black hash marks are the raw data, and the solid lines were obtained from least-squares fits of the spectrum with two doublets, *ls* component (green, 78%) δ = 0.28 mm/s and ΔE_Q = 1.70 mm/s and *hs* component (red, 22%) δ = 0.46 mm/s and ΔE_Q = 1.26 mm/s. The sample consisted of microcrystals suspended in Nujol and frozen in liquid nitrogen.

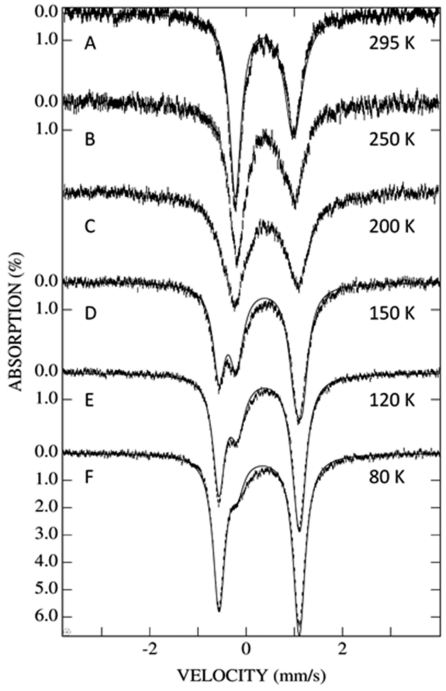

Figure 4. Variable-temperature Mössbauer spectra of **1-NN** in a 0.04 T applied magnetic field. The hash marks are the raw data, and the solid lines were obtained from least-squares fits or the spectra with two doublets with parameters in Table S3 (Supporting Information). The sample consisted of microcrystals mixed with purified adamantane powder.

the half-transition is expected to be between 160 and 180 K (see Supporting Information). At room temperature we observed an asymmetric quadrupole doublet, which was best fit with one majority species with an isomer shift of 0.38 mm/s and quadrupole splitting of 1.21 mms/s, contributing about 90% of the spectrum (second-order Doppler shift accounts for the lower isomer shift observed at room temperature). As observed by Simaan et al., the spectral decomposition in precise contributions at each temperature is complicated by temperature dependence of quadrupole splittings and line widths.[34,35] At low temperatures the spectra were well behaved, with line widths of 0.28 mm/s for the 6 and 80 K spectra and 0.30 mm/s for the 120 and 150 K spectra. The line shape was broader for the temperatures in the spin transition region and higher. At room temperature (295 K) the spectrum is asymmetric, comparable to those observed for similar [(TPA)Fe^{III}(CAT)] complexes.[34]

High-Field Mössbauer Studies. To ascertain the electronic ground states and refine our hyperfine parameters of **1-NN**, the 4.2 K spectra were collected in large applied magnetic fields of 5.0 and 7.5 T. At 4.2 K in high applied magnetic fields we observed the two components characterized in the 0.04 T spectra discussed above, both exhibiting magnetic hyperfine splitting, as expected for *ls*- and *hs*-Fe^{III} complexes. The analysis was somewhat facilitated by the fact that the low-spin spectral component has clear intense features disposed centrally (between −2 and 3 mm/s), while the high-spin component exhibits larger magnetic hyperfine splittings, spreading the more intense lines on the sides (roughly at −6 and 6 mm/s). The spectral feature of the *ls* component was fit with magnetic hyperfine coupling components of −16, −35, and −45 MHz, consistent with an S = 1/2 ground state of a low-spin ferric complex. The *ls* and *hs* components were fit separately, using spin Hamiltonians for electronic spin S = 1/2 and S = 5/2, respectively. We have also explored the possibility of a weak spin coupling with the NN radical. The best match with the experimental data is obtained with a weak *ferromagnetic* coupling with the NN radical of +5 cm^{-1} > J > +0.5 cm^{-1}. Spectral simulations are shown in Figure 5. While the sign of the coupling is clearly determined by the simulation, to ascertain the magnitude and the significance of the coupling for the electronic structure of the complex, extensive Mössbauer and EPR studies are required, which is beyond the scope of this paper.

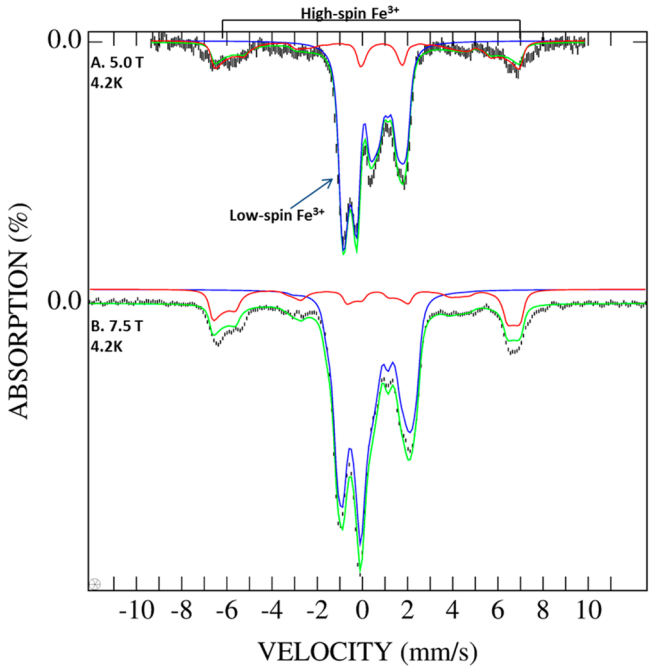

Figure 5. The 4.2 K variable-field Mössbauer spectra of complex **1-NN**. The hash marks are the raw data, and the solid lines (green solid line) were obtained from addition of the least-squares fits or the spectra for the *ls* component (81%, blue) and the *hs* component (19%, red) with the parameters in Table 1. The sample consisted of microcrystals mixed with purified adamantane powder.

DOI: 10.1021/acs.inorgchem.5b00298
Inorg. Chem. 2015, 54, 4466−4474

Table 1. Spin Hamiltonian Parameters Used to Fit the Mössbauer Spectra of the *ls* and *hs* Components of 1-NN at 4.2 K

component	δ (mm/s)	ΔE_Q (mm/s)	η	A_x, A_y, A_z (MHz)	$2J_{iso}$ (cm^{-1}; $-2JS_1S_2$)
low spin	0.29	1.22	3	−16, −35, −45	+1
high spin ($D \approx 10$ cm^{-1}, $E/D = 0.02$)	0.46	1.69	−1	−29.5, −29.5, −29.5	+1

Magnetometry. Magnetic susceptibility plots of **1** and **1-NN·MeOH** are shown in Figure 6. At room temperature, $\chi_{para}T$ for **1** is 3.82 emu K mol^{-1}, and it decreases as the temperature is decreased. Around 20 K, $\chi_{para}T$ begins to plateau at ∼1.38 emu K mol^{-1} before a sharp decrease begins at 9 K. This observed sigmoidal shape of the $\chi_{para}T$ plot, which corresponds to a SCO equilibrium, matches that reported by Funabiki et al.[12] For **1-NN·MeOH**, $\chi_{para}T$ at room temperature is 3.78 emu K mol^{-1} and, like **1**, decreases as temperature is lowered until it levels off around 20 K with a $\chi_{para}T$ value of 1.60 emu K mol^{-1}. Also like **1** a sharp decrease in susceptibility begins at 9 K. Given that a *ls*- to *hs*-Fe^{III} spin transition for **1-NN** was substantiated through variable-temperature Mössbauer and electronic absorption (vide infra) studies, the sigmoidal curvature of $\chi_{para}T$ vs T can be attributed to SCO behavior. At 300 K, $\chi_{para}T$ of **1-NN·MeOH** and **1** are within 0.040 emu K mol^{-1} of each other, and at 9 K $\chi_{para}T$ of **1-NN·MeOH** is 0.22 emu K mol^{-1} higher than **1**. Both of these $\chi_{para}T$ differences between **1-NN·MeOH** and **1** are less than the spin-only value for a monoradical substituent, suggesting exchange coupling or varied populations of metal spin state at temperature extrema.

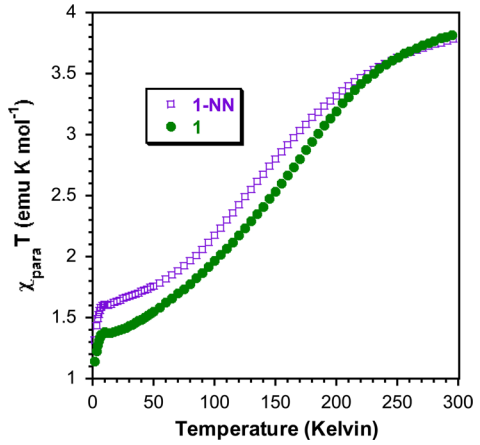

Figure 6. Paramagnetic susceptibility of **1-NN·MeOH** (purple open diamonds) and **1** (green filled circles) at 2500 G. Best fit result of SCO-weighted HDvV equation (eqs 1 and 2) of **1-NN·MeOH** shown in the Supporting Information.

To determine intramolecular exchange coupling between the metal and radical centers in **1-NN·MeOH**, a multiterm Bleaney–Bowers equation (eq 1) that incorporates ferric SCO was used.[29,22] In this expression, the first term considers intraligand exchange for the *hs*-Fe^{III} configuration, whereas the second term considers intraligand exchange for the *ls*-Fe^{III} configuration. Weighting of these terms is provided by the high-spin fraction (α_{HS}) as a function of temperature provided by eq 2. The thermodynamic parameters, H and $T_{1/2}$, applied in eq 2 were obtained from the variable-temperature electronic absorbance and Mössbauer experiments (vide infra and Supporting Information). This treatment was adapted from the work of Kahn and Teki,[29,22] but unlike their systems the SCO for **1-NN·MeOH** lacks diamagnetic species at any experimental temperature. In consideration of the high-field Mössbauer results, the magnetic susceptibility data of **1-NN·MeOH** were fit with fixed ferromagnetic J values ($J_{hs\text{-}FeIII\text{-}NN} = J_{ls\text{-}FeIII\text{-}NN} = +1$ cm^{-1}) to obtain experimentally derived thermodynamic parameters. Since these J values are weak, we also fit the data with an antiferromagnetic J set ($J_{hs\text{-}FeIII\text{-}NN} = J_{ls\text{-}FeIII\text{-}NN} = -1$ cm^{-1}) to assess fit reliability. Resulting best-fit parameters for thermodynamic values obtained were achieved with R^2 values ≥ 0.998 (see Supporting Information) with both J sets. Given the magnitudes of J values used in these fits, the exchange parameters cannot be assigned confidently through this experiment. Instead, high-field Mössbauer spectroscopy appears to be a better test for evaluating weak exchange coupling in this type of system.

$$xT = \frac{N\beta^2}{3k}\left[\alpha_{HS}\left(g_{HS}{}^2\frac{84 + 30e^{-6J_{HS}/kT}}{7 + 5e^{-6J_{HS}/kT}}\right) + (1 - \alpha_{HS})\left(g_{LS}{}^2\frac{6}{3 + e^{-2J_{LS}/kT}}\right)\right] \quad (1)$$

$$\alpha_{HS} = \frac{1}{1 + e^{(H/(RT - RT_{1/2}))}} \quad (2)$$

Absorption Spectroscopy and Cyclic Voltammetry. The electronic absorption spectra of **1-NN** and **1** are shown in Figure 7 and summarized in Table 2. Both complexes exhibit two broad features in the visible and near-IR regions. According to previous studies of ferric catecholate species, these bands are

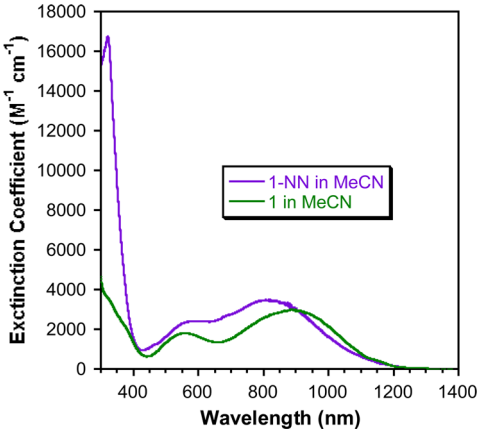

Figure 7. Electronic absorption spectra of **1-NN** (purple) and **1** (green) in MeCN.

Table 2. Electronic Absorption Spectra and Redox Potentials[a] of 1-NN and 1 in MeCN

complex	λ_{max}/nm (ε/M^{-1} cm^{-1})	E_{cp}(red)/V	$E_{1/2}$(ox$_1$)/V	E_{an}(ox$_2$)/V
1-NN	807(3485), 587(2773), 322(16 308)	−0.900	+0.173	+0.498
1	879(2915), 558(1934)	−1.053	−0.0725	+0.456

[a]See Supporting Information for cyclic voltammograms.

DOI: 10.1021/acs.inorgchem.5b00298
Inorg. Chem. 2015, 54, 4466−4474

assigned as CAT → Fe LMCT transitions.[11] The low-energy LMCT band of **1-NN** is blue-shifted by 1015 cm^{-1} relative to **1** likely due to the electron-withdrawing nature of the NN substituent.[36] The blue-shifted LMCT of **1-NN** is reflected in a 246 mV positive shift of the CAT/SQ couple of **1-NN** relative to **1** (see Supporting Information), which is commonly observed in NN-substituted dioxolene complexes.[7] The spectrum of **1-NN** contains an additional band that is absent in **1** and is assigned as a nitronylnitroxide NO $\pi \rightarrow \pi^*$ based transition on the basis of its absorption maximum and molar absorptivity.[37,38]

To further investigate Fe^{III} SCO of **1-NN**, variable-temperature electronic absorption spectra were obtained in a solid polystyrene matrix and are shown in Figure 8. At room

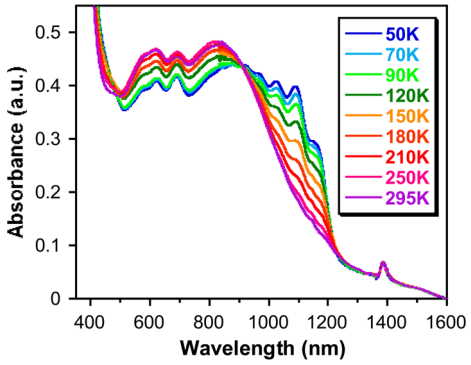

Figure 8. Variable-temperature electronic absorption spectra of **1-NN** in polystyrene. The band at 1385 nm is attributed to polystyrene.

temperature, λ_{max} of the low-energy LMCT band of **1-NN** in polystyrene is observed at 841 nm (11 891 cm^{-1}). This band is bathochromically shifted by 500 cm^{-1} relative to **1-NN** in MeCN, indicating negative solvatochromism. As the temperature is decreased, the low-energy LMCT band is bathochromically shifted by approximately 2700 cm^{-1} and adopts a vibronic progression of ~550 cm^{-1}. The observed vibronic progression resembles that of similar *ls*-Fe^{III}CAT complexes and has been assigned as a FeO_2C_2 chelate ring mode.[9,15] The spectral shift and vibronic progression corroborates SCO in **1-NN**. There is no detectable wavelength change in the higher energy LMCT band from the 50 to 295 K temperature range. Low-temperature spectra below 50 K were collected, but the spectra matched those collected at higher temperatures. This result can be attributed to a LIESST process where the *ls*-Fe^{III}CAT state is photoexcited to populate the *hs*-Fe^{III}CAT state via applied continuous NIR lamp irradiation. As shown by Enachescu et al., the metastable *hs*-Fe^{III}CAT state to *ls*-Fe^{III}CAT repopulation rate is slow and appropriate for detection with steady-state optical spectroscopy.[15]

Ultrafast Transient Absorption. The excited-state dynamics of **1** and **1-NN** were investigated through femtosecond transient absorption spectroscopy by pumping into the red side of the low-energy LMCT band (900 nm). Spectra were collected and analyzed separately in the visible and near-IR regions with short (72 ps) and long (6 ns) time scales. For **1**, transient bleaching at 546, 890, and 1300 nm was observed instantly, and bleach intensity rapidly decreased to near baseline within several picoseconds. These features correspond to ground-state LMCT bands and confirm depopulation of the *hs*-Fe^{III}CAT ground state. The transient absorption at 400 nm is also formed instantly and rapidly decays on a similar time scale as the transient bleaches. Through spectroelectrochemistry, this band was assigned as the SQ $\pi \rightarrow \pi^*$ transition (see Supporting Information), which confirms population of an Fe^{II}SQ state derived from the LMCT transition. The other transient at 1090 nm begins to emerge around 890 fs, peaks around 1.69 ps, and slowly decays on the order of several hundred picoseconds. By 30 ps, this transient band begins to demonstrate what appears to be vibronic structure similar to the FeO_2C_2 mode mentioned in the previous section. Since this band is bathochromically shifted relative to the *hs*-Fe^{III}CAT low-energy LMCT band of **1** and has vibronic structure, it was assigned as an *ls*-Fe^{III}CAT LMCT band. This suggests that an *ls*-Fe^{III}CAT state is populated following deactivation of the Fe^{II}SQ state.

Similar trends in the transient absorption spectra were observed for **1-NN**. Transient bleaching at 551, 845, and 1347 nm also occurred instantly. Like **1**, these features lost most of their intensity by several picoseconds. A positive transient at 401 nm instantly formed and decayed in a similar fashion to the transient bleaches. Like **1**, this high-energy band (at 401 nm) is assigned as the SQ $\pi \rightarrow \pi^*$ transition, as confirmed through

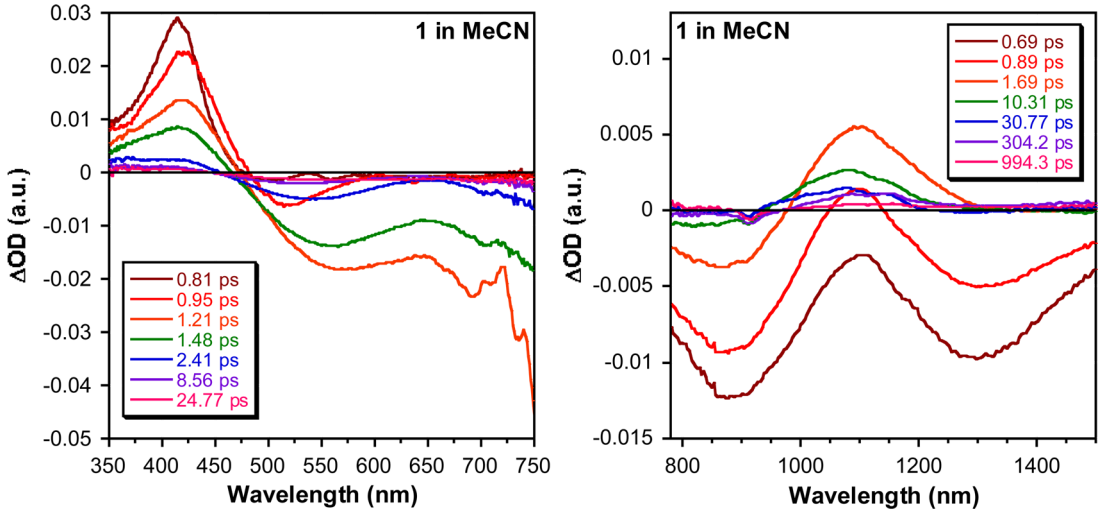

Figure 9. Visible (left) and NIR (right) transient absorption difference spectra of **1** in MeCN following 900 nm excitation.

DOI: 10.1021/acs.inorgchem.5b00298
Inorg. Chem. 2015, 54, 4466−4474

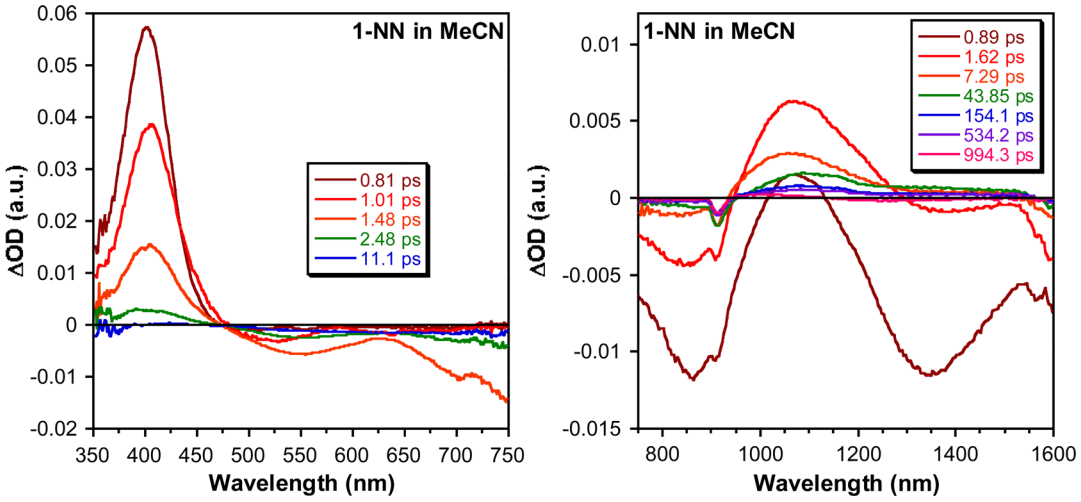

Figure 10. Visible (left) and NIR (right) transient differential spectra of **1-NN** in MeCN following 900 nm excitation.

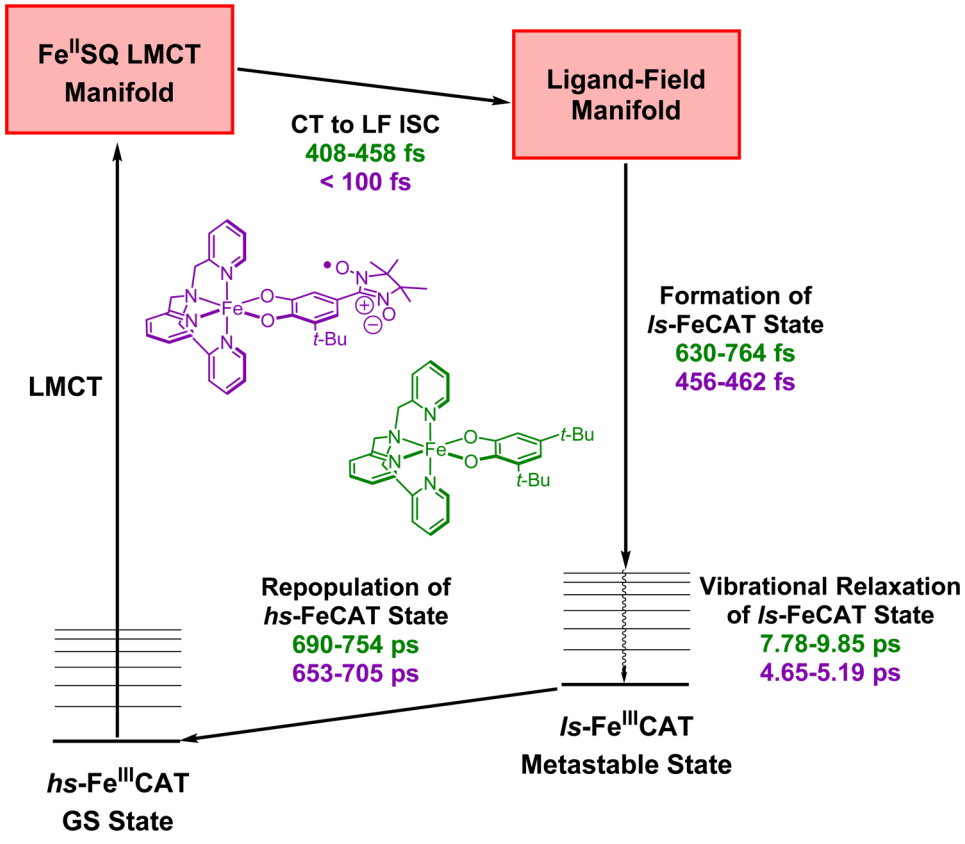

Figure 11. Jablonski diagram depicting excited states involved upon LMCT excitation of **1** and **1-NN** at room temperature in MeCN. Lifetimes in green correspond to **1**, while those in purple correspond to **1-NN**.

spectroelectrochemistry (see Supporting Information). A transient absorption observed at 1064 nm gained maximum intensity by 1.62 ps and decayed over several hundred picoseconds. This band is assigned as the low-energy *ls*-Fe^{III}CAT LMCT band since it has a λ_{max} similar to that of *ls*-Fe^{III}CAT LMCT observed through variable-temperature absorption experiments. Unlike **1**, a vibronic progression was absent in this transient spectral feature.

Through fit analysis of transient absorption features (see Supporting Information), both complexes exhibit comparable kinetics with two subpicosecond components, one fast picosecond component and one slow picosecond component. The subpicosecond decay components have lifetime ranges of 408−458 and 630−764 fs for **1** and <100[39] and 456−462 fs for **1-NN**. The fast picosecond decay component has lifetime ranges of 8−10 ps for **1** and 4−5 ps for **1-NN**. The slow decay components have lifetime ranges of 690−754 ps for **1** and 653−705 ps for **1-NN**. The positive transients associated with Fe^{II}SQ LMCT excited states for both **1** and **1-NN** decay rapidly (all within several picoseconds), and a second transient associated with an *ls*-Fe^{III}CAT state emerges within several picoseconds before decaying over hundreds of picoseconds.

DOI: 10.1021/acs.inorgchem.5b00298
Inorg. Chem. 2015, 54, 4466−4474

Given that the transitions between the $Fe^{II}SQ$ and *ls*-$Fe^{III}CAT$ states are fast (∼subpicosecond) and spin mismatch between the *ls* and *hs* states, it can be deduced that population of the ligand field (LF) manifold channels these states. It should be noted that no concrete experimental evidence for population of LF states was observed, but it is accepted that iron LF states are involved in photophysical mechanisms similar to our system.[40] At room temperature in MeCN, the relaxation dynamics of the **1-NN** complex appear to be faster than those suspected at low temperature in polystyrene. Given that both cases are believed to involve LIESST-like processes, it can be reasoned that at $T <$ 50 K the relaxation mechanism is dominated by tunneling, whereas at higher temperatures a thermally activated mechanism dominates.[15]

On the basis of our results, a Jablonski diagram has been constructed (Figure 11) for the room-temperature photophysics of both **1** and **1-NN**. Upon excitation of the LMCT band, an $Fe^{II}SQ$ state is immediately populated, which undergoes intersystem crossing to the LF manifold, where it rapidly decays into a metastable *ls*-$Fe^{III}CAT$ state. Both of these processes are less than 1 ps. Population of this metastable state (which is destabilized relative to the *hs*-$Fe^{III}CAT$ state at room temperature) is met with vibrational relaxation on the order of several picoseconds followed by repopulation of the *hs*-$Fe^{III}CAT$ ground state, which occurs over several hundred picoseconds. The fast picosecond and subpicosecond decay components of **1-NN** are notably shorter than those obtained for **1**. This is most likely due to the higher number of microstates present within the LMCT and LF manifolds for **1-NN**, which results in more pathways for population/depopulation. Even though the *ls* to *hs* repopulation for **1-NN** is also shorter relative to **1**, they are within error of each other. Since photophysics are governed by Fe-mediated processes (LF states and SCO), similarity in decay trends is observed between **1** and **1-NN**. Therefore, assessing how the strong intraligand SQ-NN exchange affects the CT states is not feasible.

CONCLUSIONS

In this work, a $[(TPA)Fe^{III}(CAT\text{-}NN)]BPh_4$ complex has been synthesized, characterized, and studied by spectroscopic methods and magnetometry. Additionally, this NN-substituted complex has been directly compared to a $(TPA)Fe^{III}$(3,5-DBCAT) complex lacking a radical fragment. For the first time, ultrafast transient absorption measurements supported by spectroelectrochemistry are reported for a $(TPA)Fe^{III}$(CAT) complex. Mössbauer spectroscopy at variable fields and temperatures provides compelling evidence for spin-crossover and ferromagnetic intramolecular exchange coupling. Ground-state absorption spectra and electrochemistry indicate a substituent effect on the electronic structure, as indicated by changes in λ_{LMCT} and redox potentials of the complexes when the pendent NN radical is attached. Variable-temperature magnetometry and electronic absorption studies indicate that the complex undergoes spin-crossover like the nonradical appended species, in agreement with our Mössbauer studies.

The photophysics of the $(TPA)Fe^{III}$(CAT) chromophore upon excitation of the low-energy LMCT band begins with population of a short-lived $Fe^{II}SQ$ state that undergoes intersystem crossing to a ligand field manifold before relaxing into a metastable *ls*-$Fe^{III}CAT$ state for both **1** and **1-NN**. The results from this study demonstrate that for this particular SCO system radicals and their photogenerated exchange-coupled fragments influence neither the SCO nor the photophysics due to competitive metal-ion-facilitated electronic processes. A possible reason for the similarity of the photophysics of the two complexes may be rooted in the extent of charge transfer in the LMCT excited state. If the charge transfer is incomplete (and little spin density resides on the dioxolene in the LMCT excited state), then the intraligand exchange coupling will be compromised and perhaps not manifest in the photophysics of the complex. To better investigate the effects of strong intraligand exchange couplings in the excited state of redox-active chromophores, designing radical-appended redox-active transition metal complexes without low-lying ligand field states and/or SCO behavior is ideal. Efforts along this line are currently under way.

EXPERIMENTAL SECTION

General Considerations. All starting reagents were obtained from commercial sources and used without further purification. Solvents also purchased from commercial sources were purified by passing through activated alumina housed in a custom-built solvent purification system. H_2CAT-NN,[6] tris(2-pyridylmethyl)amine,[41] and complex **1**[11,26] were prepared according to previous literature methods. Infrared spectra were recorded on a Brüker Vertex 80v spectrometer with a Brüker Platinum ATR attachment. Elemental analyses were performed by Atlanic Microlabs, Inc. High-resolution mass spectra were obtained at the NCSU Mass Spectrometry Facility located in the NCSU Department of Chemistry.

Magnetometry. Magnetic susceptibility and saturation plots were performed on a Quantum Design MPMS-XL SQUID magnetometer. Microcrystalline samples of approximately 20 mg were loaded into gelcap/straw holders and mounted to the sample rod with Kapton tape for both susceptibility and saturation experiments. Raw data were corrected with a straight line for the diamagnetic response of the sample holder ensemble and with Pascal's constants for molecular diamagnetic response.

Electronic Absorbance Spectroscopy. Room-temperature spectra were obtained on Shimadzu UV-1601, Shimadzu UV-1800, and Shimadzu UV-3600 spectrophotometers. Time-dependent spectra were obtained by creating an approximately 0.1 mM MeCN solution of **1-NN** in a nitrogen atmosphere glovebox in a capped 1 mm cuvette. Variable-temperature electronic absorbance (VT-Abs) spectra were collected on a Shimadzu UV-3600 UV−vis−NIR spectrophotometer. VT-Abs measurements were performed by removing the standard cuvette holder assembly to insert the Janis continuous flow cryostat with custom-designed mount. The temperature range was provided through continuous helium flow and was controlled by a Lakeshore 321 autotuning temperature controller. Samples were prepared by generation of polystyrene (MW = 280 000) polymer films from evaporation of saturated polystyrene solutions drop casted on glass microslides.

Mössbauer Spectroscopic Studies. Mössbauer spectra were recorded on two constant-acceleration spectrometers, on three samples of compound **1-NN**. Low-field (0.04 T), variable temperature (4.5−200 K) Mössbauer spectra were recorded on a closed-cycle refrigerator spectrometer (Colgate University), model CCR4K, maintaining temperatures between 4.5 and 300 K (SeeCo.us), equipped with a 0.04 T permanent magnet. High-field, variable-temperature spectra were recorded on a spectrometer cooled with liquid helium, equipped with a superconducting magnet at cryogenic temperatures, between 1.5 and 250 K (Carnegie Mellon University). Mössbauer spectra were collected on a polycrystalline powder sample (71 mg of complex **1-NN**) dispersed in freshly purified adamatane. Spectra at cryogenic temperatures were repeated on a second sample containing only 60% of the material of the first sample. A third sample was obtained by mixing the second sample with Nujol and freezing in liquid nitrogen. All sample holders were Delrin 1.00 mL cups. Thawing of samples was done in a stream of argon gas to avoid water and oxygen contamination.

DOI: 10.1021/acs.inorgchem.5b00298
Inorg. Chem. 2015, 54, 4466−4474

Mössbauer spectra were analyzed using the software WMOSS (SeeCo, formerly Web Research, Edina MN, www.SeeCo.us). Spectral simulations were elaborated in the framework of the spin Hamiltonian for electronic spins $S = 1/2$ (eq 3a, for the low-spin component) and $S = 5/2$ (eq 3b, for the high-spin component) respectively. The symbols have the standard definitions.

$$\widehat{H_{LS}} = \beta\hat{\mathbf{S}}\cdot\tilde{\mathbf{g}}\cdot\vec{\mathbf{B}} + \hat{\mathbf{S}}\cdot\tilde{\mathbf{A}}_i\cdot\hat{\mathbf{I}} + \hat{H}_Q(i) - g_n\beta_n\vec{\mathbf{B}}\cdot\hat{\mathbf{I}} \quad (3a)$$

$$\widehat{H_{HS}} = D\left[S_z^2 - \frac{1}{3}S(S+1) + \frac{E}{D}(S_x^2 - S_y^2)\right] + \beta\hat{\mathbf{S}}\cdot\tilde{\mathbf{g}}\cdot\vec{\mathbf{B}} + \hat{\mathbf{S}}\cdot\tilde{\mathbf{A}}_i\cdot\hat{\mathbf{I}} + \hat{H}_Q(i) - g_n\beta_n\vec{\mathbf{B}}\cdot\hat{\mathbf{I}} \quad (3b)$$

$$\hat{H}_Q = \frac{eQV_{zz,i}}{12}\left[\hat{I}_{z,i}^2 - \frac{15}{4} + \eta(\hat{I}_{x,i}^2 - \hat{I}_{y,i}^2)\right] \quad (4)$$

Simulations of high-field Mössbauer spectra in which exchange coupling was considered used the H_{ex} Hamiltonian, where $J < 0$ indicates that the $S = 1$ coupled state is the ground multiplet.

Transient Absorption. Ultrafast transient absorption spectra were collected on a Helios transient absorption spectrometer with a Coherent Libra-F-1K-HE Ti:sapphire amplified laser (1 kHz, 100 fs pulse width) tuned with an OPerA Solo OPA. Samples were prepared inside a glovebox with a nitrogen atmosphere. Solutions of **1** and **1-NN** in MeCN in 2 mm sealed quartz cuvettes were made so that the optical density around 900 nm was around 0.4−0.5. Time delays were controlled with a Newport motion controller model ESP301. Spectra were collected individually in the visible (307−911 nm) and NIR (747−1630 nm) regions. Additionally, spectra in both regions were collected on shorter time scales (from −10 to 72 ps) and longer time scales (−10 to 6070 ps). Each spectral set was collected with multiple scans (2 or 3 times), and the individual scans were averaged. Data were analyzed and fit using OriginPro 9.1 software. More details about kinetic fitting are available in the Supporting Information.

X-ray Diffraction. See the Supporting Information.

[(TPA)Fe(NN-Cat)]BPh_4 (1-NN). Anhydrous ferric chloride (0.09 g, 0.55 mmol) and TPA (0.16 g, 0.55 mmol) were added to a Schlenk flask. After five cycles of pump−purge, methanol (60 mL) was added followed by 2.5 h of stirring. In a separate flask, NN-Cat (0.178 g, 0.55 mmol) was also subjected to five cycles of pump−purge. Afterward, methanol (40 mL) was added followed by degassed triethylamine (0.2 mL, 1.4 mmol), and the solution was immediately added to the Schlenk flask containing ferric chloride and TPA. After stirring for another 2 h, a methanolic solution of sodium tetraphenylborate (0.29 g, 0.85 mmol), prepared in a similar fashion to that for NN-Cat, was added to the Schlenk flask. The mixture was stirred overnight and then allowed to stand for several weeks until formation of microcrystalline precipitates was observed. These precipitates were isolated as **1-NN·MeOH** (0.37 g, 66%) by vacuum filtration and washed with chilled methanol. ESI-MS (m/z): 665.25 [M^+]. Anal. Calcd for $C_{60}H_{65}BFeN_6O_5$: C, 70.87; H, 6.44; N, 8.26. Found: C, 70.50; H, 6.37; N, 8.21. IR (cm^{-1}): 3435, 3055, 2990, 1609, 1556.

■ ASSOCIATED CONTENT

Supporting Information

Crystallographic data collection details, additional structural figures, CIF file for **1-NN**, cyclic voltammograms, absorbance spectra of oxidized **1** and **1-NN**, high-spin fraction curves, attempted $\chi_{para}T$ vs T fits for **1-NN**, ultrafast transient absorption data collection and fitting details, and kinetic fit results. This material is available free of charge via the Internet at http://pubs.acs.org.

■ AUTHOR INFORMATION

Corresponding Authors

*E-mail: shulz@ncsu.edu.

*E-mail: cpopescu@colgate.edu.

Present Address

[§]Department of Chemistry, University of Western Ontario, London, Ontario, Canada.

Notes

The authors declare no competing financial interest.

■ ACKNOWLEDGMENTS

Funding for this research was provided by the National Science Foundation grants CHE-1213269 (D.A.S.) and CHE-1445959 (C.V.P.). We would like to acknowledge Dr. Evgeny Danilov and Dr. Megan Lazorski at North Carolina State University for experimental assistance. We would also like to thank Dr. Roger Sommer for helpful discussions.

■ REFERENCES

(1) Griffith, W. P. *Transition Met. Chem.* **1993**, *18*, 250−256.

(2) Costas, M.; Mehn, M. P.; Jensen, M. P.; Que, L. *Chem. Rev.* **2004**, *104*, 939−986.

(3) Best, J.; Sazanovich, I. V.; Adams, H.; Bennett, R. D.; Davies, E. S.; Meijer, A. J. H. M.; Towrie, M.; Tikhomirov, S. A.; Bouganov, O. V.; Ward, M. D.; Weinstein, J. A. *Inorg. Chem.* **2010**, *49*, 10041−10056.

(4) Shultz, D. A. Valence Tautomerism in Dioxolene Complexes of Cobalt Bistability and Hysteresis. In *Magnetism: Molecules to Materials II: Molecule-Based Materials*; Miller, J. S., Drillon, M., Eds.; Wiley-VCH: Weinheim, 2002; Vol. *4*, pp 19−27.

(5) Beni, A.; Carbonera, C.; Dei, A.; Létard, J.; Righini, R.; Sangregorio, C.; Sorace, L. *J. Braz. Chem. Soc.* **2006**, *17*, 1522−1533.

(6) Shultz, D. A.; Bodnar, S. H.; Vostrikova, K. E.; Kampf, J. W. *Inorg. Chem.* **2000**, *39*, 6091−6093.

(7) Shultz, D. A.; Vostrikova, K. E.; Bodnar, S. H.; Koo, H.; Whangbo, M.; Kirk, M. L.; Depperman, E. C.; Kampf, J. W. *J. Am. Chem. Soc.* **2003**, *125*, 1607−1617.

(8) Loughrey, J. J.; Sproules, S.; McInnes, E. J. L.; Hardie, M. J.; Halcrow, M. A. *Chem.—Eur. J.* **2014**, *20*, 6272−6276.

(9) Simaan, A. J.; Boillot, M.-L.; Carrasco, R.; Cano, J.; Girerd, J.-J.; Mattioli, T. A.; Ensling, J.; Spiering, H.; Gütlich, P. *Chem.—Eur. J.* **2005**, *11*, 1779−1793.

(10) Nakatani, N.; Hitomi, Y.; Sakaki, S. *J. Phys. Chem. B* **2011**, *115*, 4781−4789.

(11) Hitomi, Y.; Yoshida, M.; Higuchi, M.; Minami, H.; Tanaka, T.; Funabiki, T. *J. Inorg. Biochem.* **2005**, *99*, 755−763.

(12) Funabiki, T.; Fukui, A.; Hitomi, Y.; Higuchi, M.; Yamamoto, T.; Tanaka, T.; Tani, F.; Naruta, Y. *J. Inorg. Biochem.* **2002**, *91*, 151−158.

(13) Girerd, J.-J.; Boillot, M.-L.; Blain, G.; Rivière, E. *Inorg. Chim. Acta* **2008**, *361*, 4012−4016.

(14) Hauser, A. *Top. Curr. Chem.* **2004**, *234*, 155−198.

(15) Enachescu, C.; Hauser, A.; Girerd, J.-J.; Boillot, M.-L. *ChemPhysChem* **2006**, *7*, 1127−1135.

(16) "Chemical spintronics" is the study of unpaired electron spin effects on chemical phenomena.

(17) Weiss, E. A.; Chernick, E. T.; Wasielewski, M. R. *J. Am. Chem. Soc.* **2004**, *126*, 2326−2327.

(18) Teki, Y.; Matsumoto, T. *Phys. Chem. Chem. Phys.* **2011**, *13*, 5728−5746.

(19) Chernick, E. T.; Mi, Q.; Kelley, R. F.; Weiss, E. A.; Jones, B. A.; Marks, T. J.; Ratner, M. A.; Wasielewski, M. R. *J. Am. Chem. Soc.* **2006**, *128*, 4356−4364.

(20) Ito, A.; Shimizu, A.; Kishida, N.; Kawanaka, Y.; Kosumi, D.; Hashimoto, H.; Teki, Y. *Angew. Chem., Int. Ed.* **2014**, *53*, 6715−6719.

(21) Chernick, E. T.; Casillas, R.; Zirzlmeier, J.; Gardner, D. M.; Gruber, M.; Kropp, H.; Meyer, K.; Wasielewski, M. R.; Guldi, D. M.; Tykwinski, R. R. *J. Am. Chem. Soc.* **2015**, *137*, 857−863.

(22) Katayama, K.; Hirotsu, M.; Kinoshita, I.; Teki, Y. *Dalton Trans.* **2012**, *41*, 13465−13473.

(23) Katayama, K.; Hirotsu, M.; Kinoshita, I.; Teki, Y. *Dalton Trans.* **2014**, *43*, 13384−13391.

DOI: 10.1021/acs.inorgchem.5b00298
Inorg. Chem. 2015, 54, 4466−4474

(24) Kirk, M. L.; Shultz, D. A. *Coord. Chem. Rev.* **2013**, *257*, 218−233.
(25) Kirk, M. L.; Shultz, D. A.; Stasiw, D. E.; Lewis, F.; Wang, G.; Brannen, C. L.; Sommer, R. D.; Boyle, P. D. *J. Am. Chem. Soc.* **2013**, *135*, 17144−17154.
(26) Simaan, A. J.; Boillot, M.-L.; Rivière, E.; Boussac, A.; Girerd, J.-J. *Angew. Chem., Int. Ed.* **2000**, *39*, 196−198.
(27) Jang, H. G.; Cox, D. D.; Que, L. *J. Am. Chem. Soc.* **1991**, *113*, 9200−9204.
(28) Van Koningsbruggen, P. J.; Maeda, Y.; Oshio, H. *Top. Curr. Chem.* **2004**, *233*, 259−324.
(29) Sutter, J.-P.; Fettouhi, M.; Li, L.; Michaut, C.; Ouahab, L.; Kahn, O. *Angew. Chem., Int. Ed.* **1996**, *35*, 2113−2116.
(30) Jürgens, O.; Vidal-Gancedo, J.; Rovira, C.; Wurst, K.; Sporer, C.; Bildstein, B.; Schottenberger, H.; Jaitner, P.; Veciana, J. *Inorg. Chem.* **1998**, *37*, 4547−4558.
(31) Caneschi, A.; Ferraro, F.; Gatteschi, D.; Rey, P.; Sessolit, R. *Inorg. Chem.* **1990**, *29*, 1756−1760.
(32) Panthou, F. L. De; Luneau, D.; Laugier, J.; Rey, P. *J. Am. Chem. Soc.* **1993**, *115*, 9095−9100.
(33) Munck, E. *Phys. Methods Bioinorg. Chem.* **2000**, 287.
(34) Floquet, S.; Simaan, A. J.; Rivière, E.; Nierlich, M.; Thuery, P.; Ensling, J.; Gütlich, P.; Girerd, J.-J.; Boillot, M.-L. *Dalton Trans.* **2005**, 1734−1742.
(35) In the 180−250 K temperature range the spectra could not be fitted with a combination of the LS and HS components obtained at 4.2 K, signaling relaxation effects or possibly an intermediate spin complex, and additional interactions beyond the scope of the present characterization of the spin-crossover and radical coupling.
(36) Ito, A.; Kurata, R.; Sakamaki, D.; Yano, S.; Kono, Y.; Nakano, Y.; Furukawa, K.; Kato, T.; Tanaka, K. *J. Phys. Chem. A* **2013**, *117*, 12858−12867.
(37) Pütz, A.-M.; Schatzschneider, U.; Rentschler, E. *Phys. Chem. Chem. Phys.* **2012**, *14*, 1649−1653.
(38) Zoppellaro, G.; Ivanova, A.; Enkelmann, V.; Geies, A.; Baumgarten, M. *Polyhedron* **2003**, *22*, 2099−2110.
(39) First subpicosecond decay constant for **1-NN** was 36 fs, which is shorter than the excitation laser.
(40) Juban, E. A.; Smeigh, A. L.; Monat, J. E.; McCusker, J. K. *Coord. Chem. Rev.* **2006**, *250*, 1783−1791.
(41) Britovsek, G. J. P.; England, J.; White, A. J. P. *Inorg. Chem.* **2005**, *44*, 8125−8134.

DOI: 10.1021/acs.inorgchem.5b00298
Inorg. Chem. 2015, 54, 4466−4474